DC and RF characteristics of AlGaN/GaN/InGaN/GaN double-heterojunction HEMTs

Article *in* IEEE Transactions on Electron Devices · February 2007

DOI: 10.1109/TED.2006.887045 · Source: IEEE Xplore

CITATIONS
46

READS
143

6 authors, including:

Yugang Zhou
Nanjing University
26 PUBLICATIONS **792** CITATIONS
SEE PROFILE

Yong Cai
Chinese Academy of Sciences
109 PUBLICATIONS **1,829** CITATIONS
SEE PROFILE

Kei May Lau
The Hong Kong University of Science and Technology
344 PUBLICATIONS **3,986** CITATIONS
SEE PROFILE

K.J. Chen
The Hong Kong University of Science and Technology
383 PUBLICATIONS **6,114** CITATIONS
SEE PROFILE

DC and RF Characteristics of AlGaN/GaN/InGaN/GaN Double-Heterojunction HEMTs

Jie Liu, *Student Member, IEEE*, Yugang Zhou, Jia Zhu, Yong Cai, Kei May Lau, *Fellow, IEEE*, and Kevin J. Chen, *Senior Member, IEEE*

***Abstract*—We present the detailed dc and radio-frequency characteristics of an $Al_{0.3}Ga_{0.7}N/GaN/In_{0.1}Ga_{0.9}N/GaN$ double-heterojunction HEMT (DH-HEMT) structure. This structure incorporates a thin (3 nm) $In_{0.1}Ga_{0.9}N$ notch layer inserted at a location that is 6-nm away from the AlGaN/GaN heterointerface. The $In_{0.1}Ga_{0.9}N$ layer provides a unique piezoelectric polarization field which results in a higher potential barrier at the backside of the two-dimensional electron gas channel, effectively improving the carrier confinement and then reducing the buffer leakage. Both depletion-mode (D-mode) and enhancement-mode (E-mode) devices were fabricated on this new structure. Compared with the baseline AlGaN/GaN HEMTs, the DH-HEMT shows lower drain leakage current. The gate leakage current is also found to be reduced, owing to an improved surface morphology in InGaN-incorporated epitaxial structures. DC and small- and large-signal microwave characteristics, together with the linearity performances, have been investigated. The channel transit delay time analysis also revealed that there was a minor channel in the InGaN layer in which the electrons exhibited a mobility slightly lower than the GaN channel. The E-mode DH-HEMTs were also fabricated using our recently developed CF_4-based plasma treatment technique. The large-signal operation of the E-mode GaN-based HEMTs was reported for the first time. At 2 GHz, a 1×100 μm E-mode device demonstrated a maximum output power of 3.12 W/mm and a power-added efficiency of 49% with single-polarity biases (a gate bias of $+0.5$ V and a drain bias of 35 V). An output third-order interception point of 34.7 dBm was obtained in the E-mode HEMTs.**

***Index Terms*—AlGaN/GaN, depletion-mode (D-mode), double-heterojunction (DH), enhancement-mode (E-mode), HEMTs, InGaN.**

Manuscript received April 13, 2006; revised August 23, 2006. This work was supported in part by the Hong Kong Research Grant Council and National Science Foundation of China under Grant N_HKUST616/04 and a competitive earmarked Research Grant 611805. The review of this paper was arranged by Editor Y. Chan.

J. Liu and Y. Cai were with Hong Kong University of Science and Technology, Kowloon, Hong Kong. They are now with Hong Kong Applied Science and Technology Research Institute (ASTRI) Company Ltd., Kowloon, Hong Kong.

Y. Zhou was with Hong Kong University of Science and Technology, Kowloon, Hong Kong. He is now with Advanced Packaging Technology Ltd., Shanghai, Hong Kong.

J. Zhu is with Hong Kong University of Science and Technology, Kowloon, Hong Kong.

K. M. Lau and K. J. Chen are with the Department of Electrical and Electronic Engineering, Hong Kong University of Science and Technology, Kowloon, Hong Kong (e-mail: eekjchen@ust.hk).

Color versions of one or more of the figures in this paper are available online at http://ieeexplore.ieee.org.

Digital Object Identifier 10.1109/TED.2006.887045

I. Introduction

With their excellent performances in high-power operations at microwave frequencies, wide-bandgap AlGaN/GaN HEMTs are emerging as the promising candidates for next-generation RF/microwave power amplifiers. Since the first demonstration of the AlGaN/GaN HEMTs more than a decade ago [1], tremendous progresses have been made in material quality and device processing techniques, leading to much improved dc and RF performances [2]–[7]. Meanwhile, more advanced device structures are being explored for further performance improvement. For example, double-channel HEMTs [8] and composite-channel HEMTs [9], [10] have been studied for higher carrier density and improved linearity. To improve carrier confinement which could result in an improved pinch-off behavior, double-heterostructure HEMTs [11] are also being investigated. Micovic *et al.* [12] demonstrated a double heterojunction HEMTs (DH-HEMTs) with improved buffer isolation using AlGaN buffer layer with an Al composition of 4%. However, it is still difficult to obtain an AlGaN buffer layer with higher Al composition. Similar to the pseudomorphic HEMTs (PHEMTs) concept in GaAs-based HEMTs, AlGaN/InGaN/GaN HEMTs and MOSHFETs have been investigated [13], [14], with the InGaN layer serving as the channel which is confined from both sides by AlGaN and GaN. However, the crystalline quality of the InGaN layer has not been shown to reach the level of GaN layer and the highest two-dimensional electron gas (2DEG) mobility reported in the AlGaN/InGaN/GaN HEMTs is 730 $cm^2/(V \cdot s)$ [13], [14], which is significantly lower than that achieved in conventional AlGaN/GaN HEMTs. As a result, the quality of the InGaN layer has been a major hurdle which prevents it from being used as the active channel for high-performance HEMTs.

Recently, an AlGaN/GaN/InGaN/GaN HEMT structure, with an InGaN notch serving as the back-barrier [15], [16], is proposed. Instead of being used as the channel, an InGaN-notch layer was inserted at the backside of the GaN channel. Although the InGaN layer has a narrower bandgap compared with the GaN layer, the strain-induced piezoelectric polarization in the InGaN layer [17], [18] raises the potential in the InGaN layer, effectively creating a high potential barrier. This additional barrier at the backside of the channel leads to better carrier confinement and better buffer isolation, which in turn, enables improved device performance, i.e., lower buffer leakage

current and higher power gain cutoff frequency $(f_{\max})$. One order of magnitude reduction in the buffer leakage current was observed. Since the GaN layer remains as the major channel, the mobility degradation that usually occurs in InGaN layer is largely avoided.

In this paper, we provide a detailed study on the dc and RF characteristics of the AlGaN/GaN/InGaN/GaN DH-HEMT structure. The effects of In composition on the device characteristics are studied in samples with In composition of 5% and 10%, respectively. An additional benefit of the InGaN-notch samples, namely, the reduction in dislocations, is illustrated with surface morphology investigations by atomic force microscopy (AFM). This dislocation reduction leads to a reduced gate leakage current. A channel delay transit time analysis based on RF small-signal characteristics is carried out to investigate the dependence of the transit time on drain current level. It is shown that low and high current levels possess two different transit delay times, reflecting the electron mobility difference in the InGaN and GaN layers. Taking advantages of the improved power gain characteristics in DH-HEMT and a novel CF_4 plasma treatment technique we developed recently [19], enhancement-mode (E-mode) AlGaN/GaN/InGaN/GaN DH-HEMTs were fabricated to demonstrate large-signal performance close to that achieved in depletion-mode (D-mode) DH-HEMT. The cutoff frequencies of the E-mode HEMTs are comparable to those of the D-mode HEMTs. Large-signal operation of the E-mode HEMT with single-polarity gate and drain biases is also reported for the first time. An output third-order interception point (OIP3) of 34.7 dBm was obtained in the E-mode HEMT, indicating excellent linearity.

This paper is organized as follows. Section II presents the design concept of the AlGaN/GaN/InGaN/GaN DH-HEMTs with focus on the utilization of the piezoelectric polarization of the InGaN layer and the optimization of the indium composition. The details of material growth and device fabrication will be given in Section III. DC and RF small- and large-signal characteristics are presented in Section IV. Finally, we conclude in Section V.

II. Design of the AlGaN/GaN/InGaN/GaN DH-HEMT

In the conventional AlGaN/GaN HEMT structure, the 2DEG channel is located in the GaN channel layer, which is directly on the top of the GaN buffer layer. Due to the homogeneous characteristic of the GaN channel and buffer layers, the conduction band below the AlGaN barrier is continuous and rises slowly with the depth, as shown in Fig. 1(a). The conduction band profile is calculated by solving the Poisson's equation and Fermi–Dirac statistics with the polarization charges in the AlGaN layer included. Without a sharp potential barrier at the backside of the 2DEG channel, the conventional AlGaN/GaN HEMT has an intrinsic drawback: The electrons in the 2DEG channel are not confined well on the buffer side, and they can spill over to the buffer, resulting in larger buffer leakage current. Carriers in the 2DEG channel may also get their mobility reduced because of the poor confinement.

One way to improve the carrier confinement is to replace the GaN channel with certain lattice-matched or strained materials

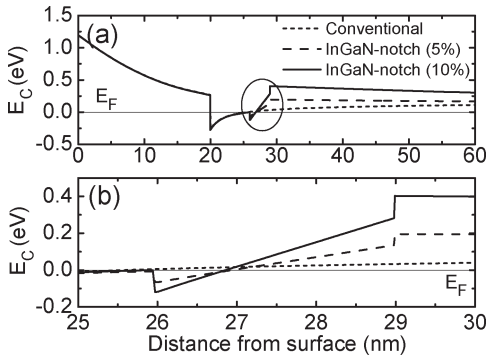

Fig. 1. (a) Calculated conduction band profiles of the conventional AlGaN/GaN HEMT and the InGaN-notch DH-HEMT. (b) Close up of the channel region. The conduction band below the channel is raised up, and a sharp potential barrier for the carriers is formed.

having a conduction band lower than GaN buffer so that the channel is confined from both sides, one side by the barrier and the other side by the buffer. One example is the PHEMT that features InGaAs channel in GaAs-based HEMTs. Naturally, there have been attempts to replace the GaN channel with InGaN layer, which features a lower conduction band than that of GaN. The biggest obstacle for this approach has been the difficulties in growing single-crystal InGaN layer and obtaining high 2DEG mobility in InGaN channel. As reported, the 2DEG mobility in this InGaN-channel HEMT structure is 730 $\mathrm{cm}^2/(\mathrm{V}\cdot\mathrm{s})$ [13], [14], which is lower than the typical value in the conventional AlGaN/GaN HEMT structure $[\sim 1000\ \mathrm{cm}^2/(\mathrm{V}\cdot\mathrm{s})]$.

On the other hand, InGaN has a strong piezoelectric polarization effect, which makes it suitable for modifying the channel structure. When a thin InGaN layer is grown in a GaN system, it is strained, and piezoelectric polarization charges could be developed accordingly. Although the InGaN layer may not be suitable for the channel without significant improvement in crystal quality, it could provide a potential barrier when it is placed between a GaN channel and GaN buffer, as shown in Fig. 1(a). Band profile simulation was carried out to optimize the position, indium composition, and thickness of the InGaN layer. The InGaN layer was chosen to be 6-nm away from the AlGaN/GaN interface. This distance is large enough to keep the majority of 2DEG still in GaN (which has higher mobility), and it is short enough for avoiding a distinctive minor channel in InGaN layer, which will result in a secondary G_m peak that degrades the device's linearity [8]. The InGaN layer thickness is chosen to be 3 nm because it can create enough potential barrier height while reducing the burden for growing thicker strained InGaN layer. The conduction band profiles of InGaN-notch DH-HEMT are plotted in Fig. 1(a), with a close-up of the InGaN layer shown in Fig. 1(b). Two indium compositions, 5% and 10%, are presented. The conduction-band offset at InGaN/GaN heterointerface and the polarization charge density in the InGaN layer are set to be $\Delta E_C =$ 0.06 and 0.12 eV, and 3.34×10^{12} and 6.68×10^{12} e/cm^2 for the 5% and 10% indium composition, respectively [17]. The structure with 10% indium shows a potential barrier height (measured from the Fermi level) of 400 meV, compared to 200 meV in the structure with 5% indium. For a comparison,

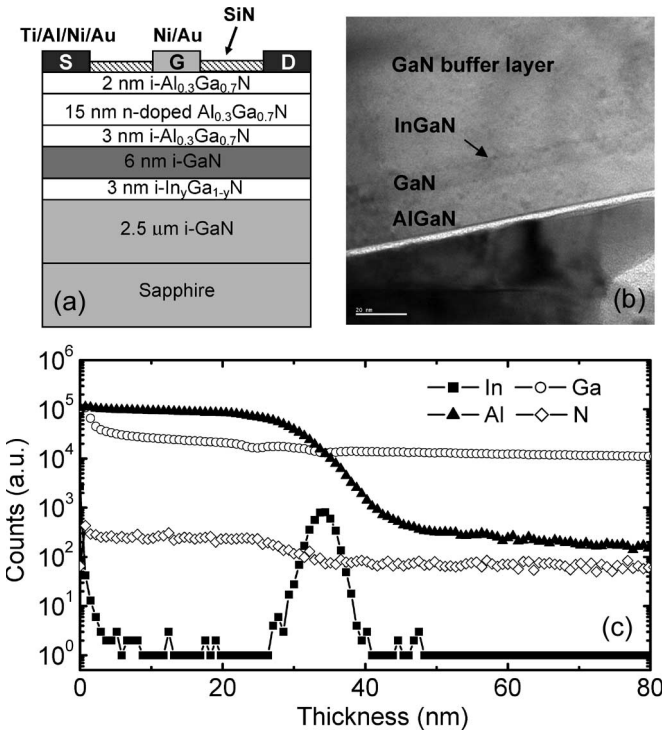

Fig. 2. (a) Cross section of the InGaN-notch DH-HEMT. A 3-nm-thick $In_yGa_{1-y}N$ ($y = 5\%$ and 10%) layer is inserted into the channel region and leaves the 6-nm-thick GaN layer to serve as the channel layer. (b) Cross-sectional TEM of the InGaN-notch DH-HEMT (10% In). A well-defined interface between the GaN channel layer and the InGaN-notch layer can be found. (c) SIMS analysis result of the InGaN-not notch DH-HEMT (10% In) wafer grown in an MOCVD system. The indium peak has an FWHM of 3.2 nm.

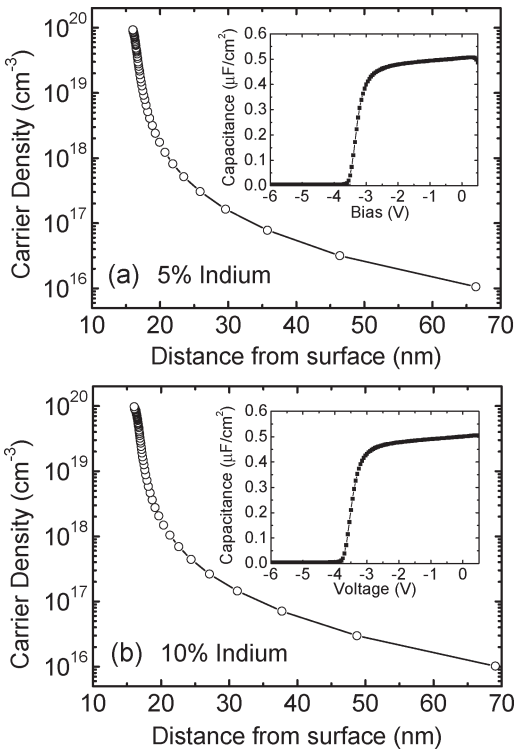

Fig. 3. C–V characteristics of the: (a) 5%-indium and (b) 10%-indium InGaN-notch DH-HEMTs, which was measured at 100 kHz on Schottky diodes fabricated on the samples. The extracted thicknesses of AlGaN barrier are about 16.5 nm, smaller than the nominal value (20 nm).

the potential barrier at the AlGaN/GaN heterointerface is 260 meV. Higher indium composition is preferred in achieving higher potential barrier and better carrier confinement. However, this indium composition implemented in practical samples must be chosen in the context of high-crystal-quality InGaN layer grown by metal–organic chemical vapor deposition (MOCVD).

III. Material Growth and Device Fabrication

A. $Al_xGa_{1-x}N/GaN/In_yGa_{1-y}N/GaN$ DH-HEMT Growth and Material Characterization

The InGaN-notch DH-HEMT structures, with the schematic cross section shown in Fig. 2(a), were grown on c-plane sapphire substrates in an Aixtron AIX 2000 HT MOCVD system. After initial desorption at 1200 °C, a GaN nucleation layer was grown at 550 °C, followed by a 2.5-μm-thick unintentionally doped GaN buffer layer grown at 1185 °C. Then, the InGaN-notch layer, which is 3-nm thick with low indium composition (5% and 10%), was grown with pure nitrogen carrier gas at 810 °C. Ammonia (NH_3), trimethyl-gallium (TMG), and trimethyl-indium (TMI) were used as the source materials. It was followed by the 6-nm-thick GaN channel layer, also grown at 810 °C. The barrier layer was grown at 1100 °C, which nominally consists of a 3-nm undoped spacer, a 15-nm doped (2×10^{18} cm^{-3}) carrier supplier layer, and a 2-nm undoped cap layer. To confirm the successful growth of the InGaN layer, material characterizations were carried out. A cross-sectional transmission-electron-microscopy (TEM) picture of the structure with 10% indium composition was taken. As shown in Fig. 2(b), a well-defined GaN/InGaN heterointerface can be found, providing direct evidence for the successful growth of the InGaN-notch layer. Fig. 2(c) shows the secondary ion mass spectroscopy (SIMS) analysis result of the sample with 10% indium. It can be found that there is an obvious indium peak with a full width at half maximum (FWHM) of 3.2 nm, which indicates that an InGaN layer was successfully grown under the GaN channel and no significant indium diffusion occurred during the subsequent high-temperature growth of the AlGaN barrier. The long tail in the Al profile is due to the stronger memory effect for Al atoms in the SIMS equipment.

To profile the carrier distribution in the InGaN-notch DH-HEMTs, capacitance–voltage (C–V) measurement was carried out on circular Schottky diodes with Schottky contact formed on top of the AlGaN barrier and the ohmic contact to the channel serving as the other electrode. The carrier distribution profiles along with the C–V characteristics of the two samples are plotted in Fig. 3. It is estimated that the carrier concentration in the AlGaN/GaN/InGaN/GaN DH-HEMT is about 9.84×10^{12} and 9.22×10^{12} cm^{-2} for 10% and 5% indium composition, respectively. Only a single peak and no plateau were observed in the carried distribution profiles, indicating that the minor channel in the InGaN layer only accommodates a small fraction of the conducting electrons and it is strongly coupled with the major GaN channel due to the small conduction band discontinuity (~120 and 60 meV above for 10% and 5% indium composition, respectively) at the GaN/InGaN

heterointerface. Since most of the electrons are in the GaN channel, the problem associated with the lower mobility of the InGaN layer was avoided. Instead, the InGaN layer plays the role of creating a potential barrier at the backside of the channel for enhanced carrier confinement. Hall measurement was performed with hall-bridge pattern fabricated on the AlGaN/GaN/InGaN/GaN DH-HEMT wafer. A 2DEG mobility of about 1300 $\mathrm{cm}^2/(\mathrm{V}\cdot\mathrm{s})$ [1230 $\mathrm{cm}^2/(\mathrm{V}\cdot\mathrm{s})$] and a sheet resistance of 480 Ω/sq (550 Ω/sq) were obtained at room temperature on the sample with 10% (5%) indium. Compared with the works employing InGaN channel layer [13], [14], the 2DEG mobility of the AlGaN/GaN/InGaN/GaN DH-HEMT is much higher [than 730 $\mathrm{cm}^2/(\mathrm{V}\cdot\mathrm{s})$]. Our baseline conventional AlGaN/GaN HEMT structure exhibits a mobility of $\sim$1100 $\mathrm{cm}^2/(\mathrm{V}\cdot\mathrm{s})$ and a sheet carrier density of 1.4×10^{13} cm^{-2}. From Fig. 3, it is also observed that the AlGaN barrier thickness in the InGaN-notch DH-HEMT samples is around 16.5 nm, smaller than the 20 nm achieved in the conventional AlGaN/GaN HEMT sample which features the same growth conditions for the AlGaN barrier. This observation indicates that the indium incorporation in the InGaN-notch DH-HEMT is most likely the factor that affects the subsequent growth of the GaN channel and AlGaN barrier. As we reported earlier [20], indium can play the role of surfactant during the growth of III-nitride materials. The thinner barriers in the DH-HEMT samples result in lower negative threshold voltages, as shown in the dc characteristics in Section IV.

B. Device Fabrication

The grown $\mathrm{Al}_x\mathrm{Ga}_{1-x}\mathrm{N/GaN/In}_y\mathrm{Ga}_{1-y}\mathrm{N/GaN}$ DH-HEMT epilayer was used to fabricate both D- and E-mode devices. Detailed description of the fabrication procedures has been given in [15] and [19]. Device active regions were defined using a 300-nm-thick mesa etching by Cl_2-based inductively coupled plasma reactive ion etching (ICP-RIE). It is followed by the source/drain ohmic contacts formation by a rapid thermal annealing (RTA) of e-beam evaporated Ti/Al/Ni/Au multilayer at 850 °C for 30 s. Using on-wafer transfer length method patterns, the ohmic contact resistance was typically measured to be 0.8 $\Omega\cdot$mm. The gates of the D- and E-mode HEMTs were processed in two separate steps. First, gate electrodes of the D-mode HEMTs with 1-μm length were defined by contact photolithography, Ni/Au e-beam evaporation, and lift-off, subsequently. The devices have a source–gate spacing of $L_{\mathrm{sg}} = 1$ μm and a gate-drain spacing of $L_{\mathrm{gd}} = 1$ μm. For the E-mode devices, after defining the gate electrode windows by photolithography and before the deposition of the gate metal, the sample was treated by CF_4 plasma in an RIE system at an RF plasma power of 150 W for 150 s. After Ni/Au e-beam evaporation and lift-off, a postgate RTA was conducted at 400 °C for 10 min. Finally, SiN was deposited on the sample by plasma-enhanced CVD for device passivation.

IV. Device Characteristics

A. DC Characteristics

The dc transfer characteristics I_{DS}–V_{GS} and transconductance (G_m) of the D-mode AlGaN/GaN/InGaN/GaN DH-HEMTs are plotted and compared with those of the conventional AlGaN/GaN HEMT in Fig. 4. The gate dimension of the devices is 1×10 μm. The threshold voltage of the D-mode DH-HEMT with 5% and 10% indium composition is -3.6 and -3.8 V, respectively, which is higher than that of the conventional HEMT (-4.7 V). This difference is caused by the different barrier thicknesses between the DH-HEMT samples and the conventional HEMT sample. The maximum drain current of the DH-HEMT is about 800 mA/mm, which is lower than the conventional one ($\sim$900 mA/mm) due to a smaller 2DEG density. It is found that the DH-HEMT shows a smaller OFF-state leakage current than the conventional one. For the DH-HEMT with a 10% indium composition, the leakage current is about 5 μA/mm at $V_{\mathrm{DS}} = 10$ V and $V_{\mathrm{GS}} < -4$ V, significantly lower than that in our conventional HEMT devices ($\sim$20 μA/mm at $V_{\mathrm{GS}} = -5.2$ V and $\sim$45 μA/mm at $V_{\mathrm{GS}} = -8$ V). For the 5% indium DH-HEMT, the leakage current is about 10 μA/mm, which is smaller than the conventional HEMT but larger than the 10% indium DH-HEMT. The different leakage currents in the two DH-HEMTs are due to the difference in the barrier height at the backside of 2DEG channel, as shown in Fig. 1(b). The reduced leakage current in the DH-HEMTs strongly indicates that the potential barrier provided by the inserted InGaN layer below the 2DEG channel can effectively improve the buffer isolation and an indium composition of 10% is more efficient than 5% indium. The peak transconductance of the DH-HEMT is about 225 mS/mm (for 10% indium) and 215 mS/mm (for 5% indium), which is about 10% and 5% higher than that in our conventional HEMT devices ($\sim$205 mS/mm). The differences in G_m's of the conventional HEMT and DH-HEMTs originate from the incorporation of indium during the growth of the AlGaN barrier layer, which was found to slow down the growth rate of AlGaN. A reduced AlGaN barrier thickness results in a smaller gate-to-channel distance, yielding higher peak transconductances.

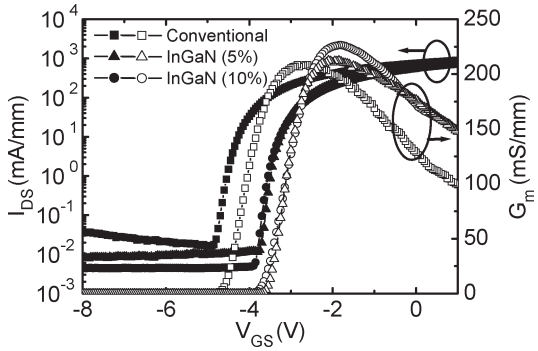

Fig. 4. DC transfer characteristics of the InGaN-notch DH-HEMTs, compared with the conventional one.

The current–voltage $(I$–$V)$ characteristics of the gate-to-drain Schottky diode were also investigated. The results are plotted in Fig. 5(a). The DH-HEMT devices exhibited a lower reverse gate leakage current, which is about 75% lower than that of the conventional HEMT. The reduced gate leakage current in the InGaN-notch structures is a result of the improved surface morphology and the dislocation reduction. As shown in the AFM results in Fig. 5(b) and (c), the line-shape dislocations that are usually observed in the conventional

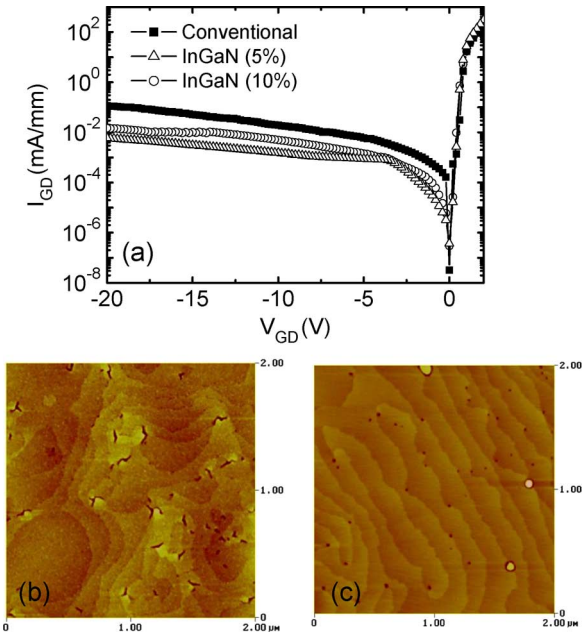

Fig. 5. (a) DC $I_{\rm GD}$–$V_{\rm GD}$ characteristics of the DH-HEMTs and the conventional HEMT. AFM pictures of: (b) conventional HEMTs and (c) DH-HEMTs (10% In). Lower dislocation density was achieved on the DH-HEMTs.

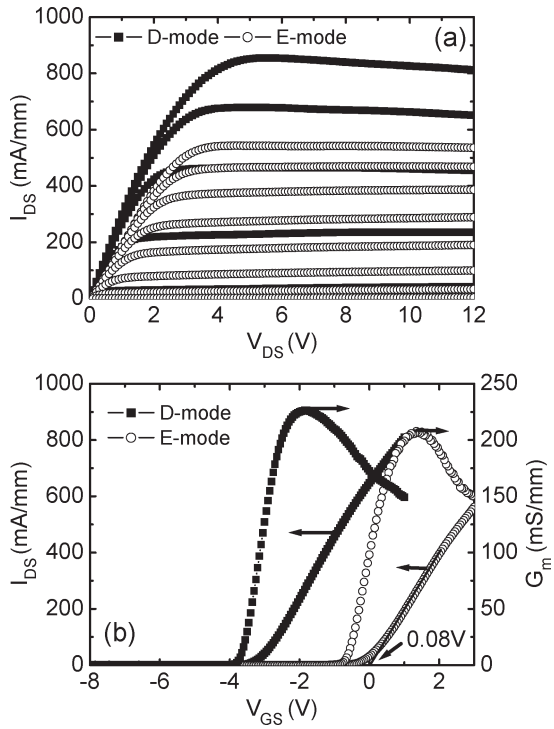

Fig. 6. DC characteristics of the D-mode (square) and E-mode (circle) InGaN-notch DH-HEMT devices. (a) $I_{\rm DS}$–$V_{\rm DS}$ curves. For the D-mode HEMT, $V_{\rm GS}$ starts from $+1$ V at the top with a step of -1 V. For the E-mode HEMT, $V_{\rm GS}$ starts from $+3$ V with a step of -0.5 V. (b) $I_{\rm DS}$–$V_{\rm GS}$ and G_m–$V_{\rm GS}$ curves, where the D-mode device showed a threshold voltage of -3.8 V and the E-mode device showed a threshold voltage of $+0.08$ V.

[Fig. 5(b)] AlGaN/GaN structures are absent in the InGaN-notch [Fig. 5(c)] samples. As reported recently [20], indium atoms can play the role of surfactant and reduce the dislocation density effectively. Although the indium source is only turned on during the growth of the InGaN-notch layer, it is likely that a small fraction of the indium atoms play the role of surfactant and accompany the moving surface all the way up to the AlGaN layer in the subsequent growth of the GaN channel and AlGaN barrier. The DH-HEMTs with 5% and 10% indium composition have similar surface morphology, and both can exhibit reduced gate leakage current. Since the DH-HEMT with 10% indium exhibits the lowest buffer leakage and the highest transconductance, this sample is the focus of the study for high-frequency small- and large-signal characterizations and E-mode HEMT characterization.

Fig. 6 shows the comparison of the $I_{\rm DS}$–$V_{\rm DS}$ and $I_{\rm DS}$–$V_{\rm GS}$ curves of 1×10 μm D- and E-mode devices fabricated on the DH-HEMT structure with $In_{0.1}Ga_{0.9}N$-notch. After CF_4 plasma treatment and postgate annealing [19], the threshold voltage of the DH-HEMT device was shifted from -3.8 to $+0.08$ V. As shown in Fig. 6(b), with a gate bias of $+3$ V, the maximum drain current on this E-mode DH-HEMT device is about 540 mA/mm, which is about 66% of the value of the D-mode devices. The peak value of the transconductance of this device, as shown in Fig. 6(b), is about 210 mS/mm, which is comparable to its D-mode counterpart (225 mS/mm).

B. Small-Signal RF Characteristics of the E-Mode DH-HEMT

Bias-dependent small-signal S-parameters measurements were conducted on 1×100 μm D- and E-mode AlGaN/GaN/$In_{0.1}Ga_{0.9}N$/GaN DH-HEMTs, using an HP 4142B modular dc source/monitor and an Agilent 8722ES network analyzer with cascade microwave probes. At a fixed source–drain bias of 10 V, the current gain ($|h_{21}|^2$) and the maximum available/stable power gain (MAG/MSG) were extracted and plotted in Fig. 7(a), with the gate biased at -1.5 V for the D-mode device and $+1$ V for the E-mode device, respectively. The D-mode (E-mode) DH-HEMT devices exhibited a current gain cutoff frequency (f_T) of 14.5 GHz (14.9 GHz) and a power gain cutoff frequency ($f_{\rm max}$) of 45.4 GHz (46.2 GHz). Fig. 7(b) shows the f_T and $f_{\rm max}$ versus drain current for the D- and E-mode devices.

Compared with our conventional AlGaN/GaN HEMT devices, the DH-HEMT devices have a similar f_T but a higher $f_{\rm max}$ value [15]. This can be attributed to the lower buffer leakage in the DH-HEMT devices. Lower buffer leakage will result in larger output resistance of the devices. In the first-order approximation, $f_{\rm max}$ is related to f_T in the following equation [21]:

$$\frac{f_{\rm max}}{f_T} = \frac{1}{2}\left(\frac{R_{\rm ds}}{R_g + R_i}\right)^{1/2}$$

where $R_{\rm ds}$, R_g, and R_i are the output resistance, gate parasitic resistance, and charging resistance of the device, respectively. With a larger $R_{\rm ds}$, the DH-HEMT devices will have a higher $f_{\rm max}$ than the conventional ones. The output resistance of the D-mode AlGaN/GaN/$In_{0.1}Ga_{0.9}N$/GaN DH-HEMT device and our conventional HEMT device were extracted from the S-parameters measured at 2 GHz based on the equivalent circuit model shown in Fig. 8, and the results are plotted together

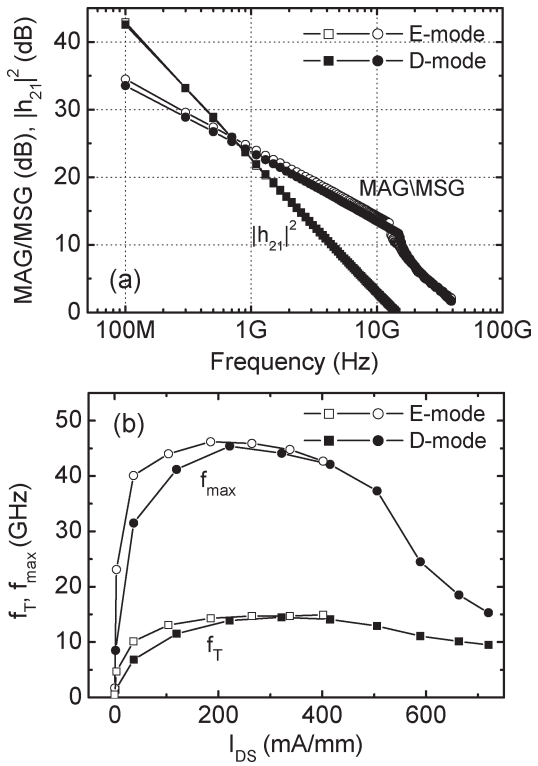

Fig. 7. RF small-signal characteristics of 1×100 μm D-mode (square) and E-mode (circle) InGaN-notch DH-HEMT devices. (a) Frequency-dependent $|h_{21}|^2$ and MAG/MSG curves extracted from the measured S-parameters. The drain bias is 10 V, and the gate bias is chosen at the point when maximum f_T is obtained. (b) Bias-dependent f_T and $f_{\max}$ curves with the source-to-drain voltage $V_{\rm DS}$ fixed at 10 V.

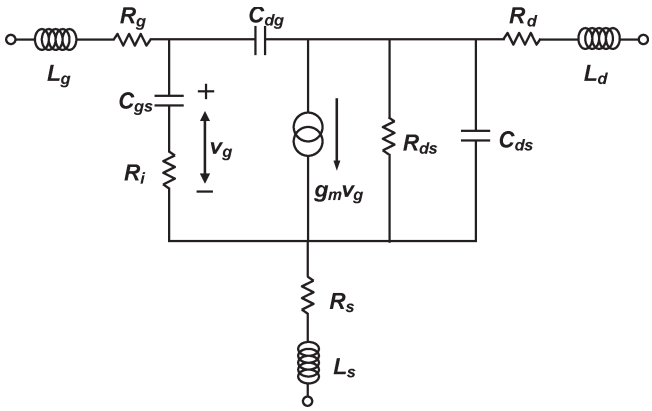

Fig. 8. Equivalent small-signal circuit model for HEMTs.

in Fig. 9. It can be found the DH-HEMT devices have a $R_{\rm ds}$ larger than that of the conventional one.

To evaluate the channel transport properties of the InGaN-notch DH-HEMT, the bias-dependent transit delay time were extracted and plotted against $1/I_{\rm DS}$ in Fig. 10. By extrapolating the linear part of the curve at low current levels to the infinite drain current, the channel transit delay time can be obtained from the interception with the time axis [22]. Unlike the conventional HEMT which features a single well-defined transit delay time [22], two values of transit delay time can be obtained from the InGaN-notch DH-HEMT. As shown in Fig. 10, there are two linear parts with different slops, which result in a channel delay time of 8.9 and 9.9 ps. The smaller delay time

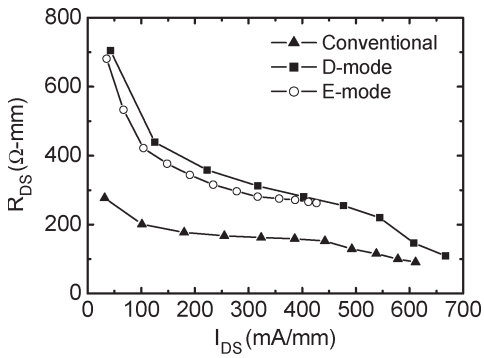

Fig. 9. Bias-dependent output resistance ($R_{\rm DS}$) curves extracted from on-wafer S-parameter measurements (frequency $= 2$ GHz) for 1×100 μm D-mode InGaN-notch DH-HEMT (circle) and conventional HEMT (square) devices.

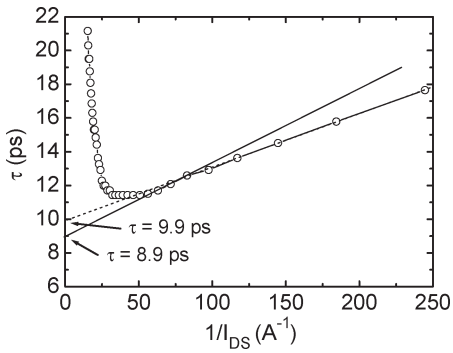

Fig. 10. Channel transit delay characteristics of the InGaN-notch DH-HEMT (10% In). Two different channel transit delay times (8.9 and 9.9 ps) were obtained on the DH-HEMT.

is obtained at relatively high current level, corresponding to the situation when majority of electrons are located in the major channel in GaN, which has a higher 2DEG mobility, while the larger delay time is obtained at low current level, when most of the electrons are located in the minor channel in the InGaN layer. Although a well-defined heterointerface can be found between GaN/InGaN by TEM, the crystal quality of the InGaN layer is not good enough and causes mobility degradation, which resulted in a larger channel transit delay time. This observation justifies our intention of using the InGaN layer at the backside of the channel for enhanced barrier confinement, instead of using it as the channel.

C. Large-Signal RF Characteristics: Power and Linearity

Large-signal load pull measurements were conducted on both the D- and E-mode DH-HEMT devices at 2 GHz using a Maury load-pull system. By tuning the input and output impedance for maximum output power, a linear gain of 25.5 dB (26 dB) together with a power density of 3.45 W/mm (3.12 W/mm) and a power-added efficiency (PAE) of 44% (49%) were obtained with a 35-V drain supply voltage on a 1×100 μm D-mode (E-mode) device, as shown in Fig. 11. The substrates were not thinned down, and no cooling treatment was employed in the measurements. The maximum output power density of the E-mode DH-HEMT is comparable with the value of its D-mode counterpart fabricated on the same wafer. To the best of our

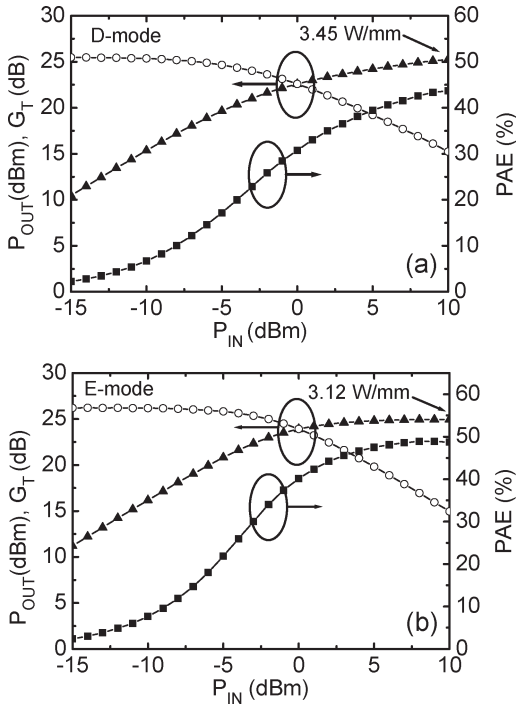

Fig. 11. Power performances of 1×100 μm (a) D-mode and (b) E-mode InGaN-notch DH-HEMT devices measured at 2 GHz, with a drain supply voltage of 35 V. For the D-mode one, $V_{\rm GS} = -2.5$ V, $G_{\rm Linear} = 25.5$ dB, $P_{\rm out,max} = 3.45$ W/mm, and maximum PAE $= 44\%$. For the E-mode one, $V_{\rm GS} = +0.5$ V, $G_{\rm Linear} = 26$ dB, $P_{\rm out,max} = 3.12$ W/mm, and maximum PAE $= 49\%$.

knowledge, this is the first large-signal power characteristics reported on the E-mode GaN-based HEMT devices.

To investigate the current collapse issue of the DH-HEMTs, dynamic I–V characteristics were measured using an Accent DIVA D265 dynamic I–V analyzer. The results are shown in Fig. 12. The pulsewidth is 1 μS and the pulse separation is 1 mS. The drain bias is 10 V, and the gate bias is -2.5 and $+0.5$ V for the D- and E-mode DH-HEMTs, respectively. No significant dc-to-pulse dispersion was found for both the D- and E-mode DH-HEMTs.

To characterize the linearity of the DH-HEMT devices, two-tone third order intermodulation (IM3) was measured at 2 GHz with an offset frequency of 1 MHz. The result is plotted in Fig. 13. An OIP3 of 29.2 and 34.7 dBm were obtained on 1×100 μm D- and E-mode DH-HEMT devices, respectively.

V. Conclusion

In this paper, a detailed investigation on the $Al_{0.3}Ga_{0.7}N/GaN/In_{0.1}Ga_{0.9}N/GaN$ DH-HEMTs is presented. By inserting a thin $In_{0.1}Ga_{0.9}N$ layer into the channel region of our conventional $Al_{0.3}Ga_{0.7}N/GaN$ HEMT structure, a sharp potential barrier was formed under the 2DEG channel, which can help in improving the carrier confinement and then improving the buffer isolation characteristics. One order of magnitude lower buffer leakage current was achieved on the InGaN-notch DH-HEMTs with 10% indium composition compared with our conventional $Al_{0.3}Ga_{0.7}N/GaN$ HEMTs. The lower buffer leakage current features a larger output resistance of the

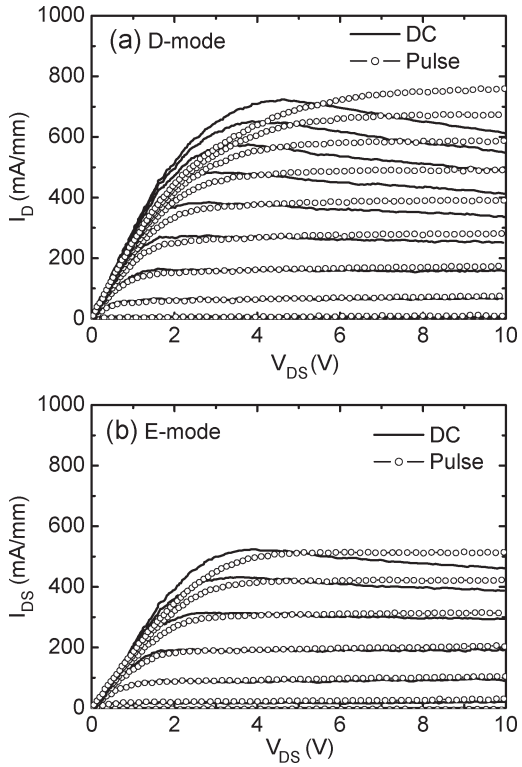

Fig. 12. DC (straight line) and pulsed (circle) I–V characteristics of the: (a) D-mode and (b) E-mode DH-HEMTs. For the D-mode one, $V_{\rm GS}$ starts from $+1$ V with a step of -1 V, and the starting biases for the pulses are: $V_{\rm DS} = 10$ V and $V_{\rm GS} = -2.5$ V. For the E-mode one, $V_{\rm GS}$ starts from $+2.5$ V with a step of -0.5 V, and the starting biases for the pulses are: $V_{\rm DS} = 10$ V and $V_{\rm GS} = +0.5$ V. The pulsewidth is 1 μs, and the pulse separation is 1 ms.

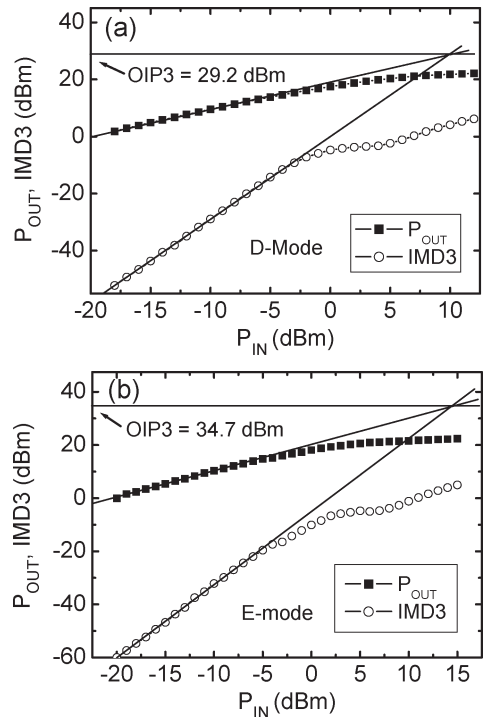

Fig. 13. IM3 measurement results of 1×100 μm (a) D-mode and (b) E-mode InGaN-notch DH-HEMT devices with a fundamental frequency of 2 GHz and an offset frequency of 1 MHz. An OIP3 of 29.2 and 34.7 dBm were obtained on the D-mode and E-mode device, respectively.

devices and results in a higher cutoff frequency of the power gain. Compared to the $Al_xGa_{1-x}N/In_yGa_{1-y}N/GaN$ HEMTs where the channel layer is $In_yGa_{1-y}N$, the InGaN-notch DH-HEMTs relaxes the requirement of growing a high-quality cluster-free $In_yGa_{1-y}N$ channel layer, which normally has a lower 2DEG mobility due to the poor crystal quality.

E-mode devices with good dc, RF small signal, and power performances were realized on the InGaN-notch DH-HEMT structure by CF_4 plasma treatment before the deposition of the gate electrodes. The threshold voltage was shifted by about 4 V. An output power density of 3.12 W/mm together with a PAE of 49% were first reported on a 1×100 μm E-mode GaN-based device.

REFERENCES

[1] M. A. Khan, J. M. Van Hove, J. N. Kuznia, and D. T. Olsen, "High electron mobility GaN–AlGaN heterostructures grown by LPMOCVD," *Appl. Phys. Lett.*, vol. 58, no. 21, pp. 2408–2410, May 1991.

[2] U. K. Mishra, P. Parikh, and Y. F. Wu, "AlGaN/GaN HEMTs—An overview of device operation and applications," *Proc. IEEE*, vol. 90, no. 6, pp. 1022–1031, Jun. 2002.

[3] K. Kasahara, N. Miyamoto, Y. Ando, Y. Okamoto, T. Nakayama, and M. Kuzuhara, "Ka-band 2.3 W power AlGaN/GaN heterojunction FET," in *IEDM. Tech. Dig.*, Dec. 2002, pp. 667–680.

[4] K. Joshin, T. Kikkawa, H. Hayashi, S. Yokogawa, M. Yokoyama, N. Adachi, and M. Takikawa, "A 174 W high-efficiency GaN HEMT power amplifier for W-CDMA base station applications," in *IEDM Tech. Dig.*, Dec. 2003, pp. 983–985.

[5] Y. F. Wu, A. Saxler, M. Moore, R. P. Smith, S. Sheppard, P. M. Chavarkar, T. Wisleder, U. K. Mishra, and P. Parikh, "30-W/mm GaN HEMTs by field plate optimization," *IEEE Electron Device Lett.*, vol. 25, no. 3, pp. 117–119, Mar. 2004.

[6] M. Kanamura, T. Kikkawa, and K. Joshin, "A 100-W high-gain AlGaN/GaN HEMT power amplifier on a conductive N–SiC substrate for wireless base station applications," in *IEDM Tech. Dig.*, Dec. 2004, pp. 799–802.

[7] Y. F. Wu, M. Moore, T. Wisleder, P. M. Chavarkar, U. K. Mishra, and P. Parikh, "High-gain microwave GaN HEMTs with source-terminated field-plates," in *IEDM Tech. Dig.*, Dec. 2004, pp. 1078–1079.

[8] R. M. Chu, Y. G. Zhou, J. Liu, D. Wang, K. J. Chen, and K. M. Lau, "AlGaN–GaN double-channel HEMTs," *IEEE Trans. Electron Devices*, vol. 52, no. 4, pp. 438–446, Apr. 2005.

[9] J. Liu, Y. G. Zhou, R. M. Chu, Y. Cai, K. J. Chen, and K. M. Lau, "$Al_{0.3}Ga_{0.7}N/Al_{0.05}Ga_{0.95}N$/GaN composite-channel HEMTs with enhanced linearity," in *IEDM Tech. Dig.*, Dec. 2004, pp. 811–814.

[10] ——, "Highly linear $Al_{0.3}Ga_{0.7}N/Al_{0.05}Ga_{0.95}N$/GaN composite-channel HEMTs," *IEEE Electron Device Lett.*, vol. 26, no. 3, pp. 145–147, Mar. 2005.

[11] N. Maeda, T. Saitoh, K. Tsubaki, T. Nishida, and N. Kobayashi, "Enhanced effect of polarization on electron transport properties in AlGaN/GaN double-heterostructure field-effect transistors," *Appl. Phys. Lett.*, vol. 76, no. 21, pp. 3118–3120, May 2000.

[12] M. Micovic *et al.*, "GaN double heterojunction field effect transistor for microwave and millimeterwave power applications," in *IEDM Tech. Dig.*, Dec. 2004, pp. 807–810.

[13] G. Simin, X. Hu, A. Tarakji, J. Zhang, A. Koudymov, S. Saygi, J. Yang, M. A. Khan, M. Shur, and R. Gaska, "AlGaN/InGaN/GaN double heterostructure field-effect transistor," *Jpn. J. Appl. Phys.*, vol. 40, no. 11A, pp. L1142–L1144, Nov. 2001.

[14] G. Simin, A. Koudymov, H. Fatima, J. Zhang, J. Yang, M. A. Khan, X. Hu, A. Tarakji, R. Gaska, and M. Shur, "SiO2/AlGaN/InGaN/GaN MOSDHFETs," *IEEE Electron Device Lett.*, vol. 23, no. 8, pp. 458–460, Aug. 2002.

[15] J. Liu, Y. G. Zhou, J. Zhu, K. M. Lau, and K. J. Chen, "AlGaN/GaN/InGaN/GaN double heterojunction HEMTs with an InGaN-notch for enhanced carrier confinement," *IEEE Electron Device Lett.*, vol. 27, no. 1, pp. 10–12, Jan. 2006.

[16] T. Palacios, A. Chakraborty, S. Heikman, S. Keller, S. P. DenBaars, and U. K. Mishra, "AlGaN/GaN high electron mobility transistors with InGaN back-barriers," *IEEE Electron Device Lett.*, vol. 27, no. 1, pp. 13–15, Jan. 2006.

[17] O. Ambacher *et al.*, "Pyroelectric properties of Al(In)GaN/GaN hetero- and quantum well structures," *J. Phys.: Condens. Matter*, vol. 14, no. 13, pp. 3399–3434, 2002.

[18] H. Zhang, E. J. Miller, E. T. Yu, C. Poblenz, and J. S. Speck, "Measurement of polarization charge and conduction-band offset at $In_xGa_{1-x}N$ heterojunction interfaces," *Appl. Phys. Lett.*, vol. 84, no. 23, pp. 4644–4646, Jun. 2004.

[19] Y. Cai, Y. G. Zhou, K. J. Chen, and K. M. Lau, "High-performance enhancement-mode AlGaN/GaN HEMTs using fluoride-base plasma treatment," *IEEE Electron Device Lett.*, vol. 26, no. 7, pp. 435–437, Jul. 2005.

[20] Z. H. Feng, S. J. Cai, K. J. Chen, and K. M. Lau, "Isoelectronic indium-surfactant-doped $Al_{0.3}Ga_{0.7}N$/GaN high electron mobility transistors," *Appl. Phys. Lett.*, vol. 88, p. 122 113, 2006.

[21] J. M. Golio, *Microwave MESTETs & HEMTs*. Boston, MA: Artech House, 1991, p. 299.

[22] M. Akita, S. Kishimoto, K. Maezawa, and T. Mizutani, "Evaluation of effective electron velocity in AlGaN/GaN HEMTs," *Electron. Lett.*, vol. 36, no. 20, pp. 1736–1737, Sep. 2000.

Jie Liu (S'00) received the B.S. and M.S. degrees in physics from Nanjing University, Nanjing, China, in 2000 and 2003, respectively, and the Ph.D. degree in electrical and computer engineering from the Hong Kong University of Science and Technology (HKUST), Kowloon, Hong Kong, in 2006. His M.S. thesis was on the Schottky contacts of III-nitride devices.

In August 2003, he joined Prof. K. Chen's group at HKUST, working on device technologies and high-frequency characterization techniques of III-nitride HEMTs. In particular, he focused on the channel engineering of III-nitride HEMTs and developed highly linear composite-channel HEMT and low-leakage current AlGaN/GaN/InGaN/GaN DH-HEMT. In October 2006, he joined the Hong Kong Applied Science and Technology Research Institute (ASTRI) Company Ltd., Kowloon, working on advanced wireless packaging technologies.

Yugang Zhou was born in Hubei Province, China, in 1975. He received the B.S. and the Ph.D. degrees from the Department of Physics, Nanjing University, Nanjing, China, in 1996 and 2001, respectively.

From September 2001 to September 2004, he was a Postdoctoral Research Associate with the Department of Electrical and Electronic Engineering, Hong Kong University of Science and Technology, Kowloon, Hong Kong. In September 2004, he joined Advanced Packaging Technology Ltd., Shanghai, Hong Kong. He mainly worked on MOCVD growth, device fabrication, and device physics of GaN-based heterojunction FETs before September 2004. After that, he focused on the fabrication of GaN based on high-power LED.

Jia Zhu, photograph and biography not available at the time of publication.

Yong Cai was born in Nanjing, Jiangsu Province, China, in 1971. He received the B.S. degree from the Department of Electronics Engineering, Southeast University, Nanjing, China, in 1993 and the Ph.D. degree from the Institute of Microelectronics, Peking University, Beijing, China, in 2003.

From 2003 and 2006, he was a Postdoctoral Research Associate with the Department of Electronic and Computer Engineering, Hong Kong University of Science and Technology, Kowloon, Hong Kong, working on wide bandgap GaN-based devices and circuits. In August 2006, he joined the Material and Packing Technologies Group of Hong Kong Applied Science and Technology Research Institute (ASTRI) Company Ltd., Kowloon, as a Senior Engineer.

Kei May Lau (S'78–M'80–SM'92–F'01) received the B.S. and M.S. degrees in physics from the University of Minnesota, Minneapolis, in 1976 and 1977, respectively, and the Ph.D. degree in electrical engineering from Rice University, Houston, TX, in 1981.

From 1980 to 1982, she was a Senior Engineer with the M/A-COM Gallium Arsenide Products, Inc., where she worked on epitaxial growth of GaAs for microwave devices, development of high-efficiency and millimeterwave IMPATT diodes, and multiwafer epitaxy by the chloride transport process. In the fall of 1982, she joined the faculty of the Electrical and Computer Engineering Department, University of Massachusetts (UMass), Amherst, where she became a full professor in 1993. She initiated MOCVD and compound semiconductor materials and devices programs at UMass. Her research group performed studies on heterostructures, quantum wells, strained-layers, III–V selective epitaxy, as well as high-frequency and photonic devices. She spent her first sabbatical leave in 1989 at the Massachusetts Institute of Technology Lincoln Laboratory. She developed acoustic sensors at the DuPont Central Research and Development Laboratory, Wilmington, DE, during her second sabbatical leave (1995–1996). In the fall of 1998, she was a Visiting Professor with the Hong Kong University of Science and Technology (HKUST), Kowloon, Hong Kong, where she joined the regular faculty since the summer of 2000. She established the Photonics Technology Center for R&D efforts in wide-gap semiconductor materials and devices. She became a Chair Professor of electrical and electronic engineering with HKUST in July 2005.

Dr. Lau was a recipient of the National Science Foundation (NSF) Faculty Awards for Women (FAW) Scientists and Engineers. She served on the IEEE Electron Devices Society Administrative Committee and was an Editor of the IEEE TRANSACTIONS ON ELECTRON DEVICES (1996–2002). She also served on the Electronic Materials Committee of the Minerals, Metals and Materials Society (TMS) of the American Institute of Materials Engineers (AIME).

Kevin J. Chen (M'95–SM'06) received the B.S. degree from the Department of Electronics, Peking University, Beijing, China, in 1988 and the Ph.D. degree from the University of Maryland, College Park, in 1993.

From January 1994 to December 1995, he was a Research Fellow with the NTT LSI laboratories, Atsugi, Japan, engaging in the research and development of functional quantum effect devices and heterojunction FETs (HFETs). In particular, he developed the device technologies for monolithic integration of resonant tunneling diodes and HFETs (MISFET and HEMT) on both GaAs and InP substrates, for applications in ultrahigh-speed signal processing and communication systems. He also developed the Pt-based buried gate technology that is widely used in the E-mode HEMT and PHEMT devices. From 1996 to 1998, he was an Assistant Professor with the Department of Electronic Engineering, City University of Hong Kong, carrying out research on high-speed device and circuit simulations. He then joined the wireless semiconductor division of Agilent Technologies, Inc., Santa Clara, CA, in 1999, working on E-mode PHEMT RF power amplifiers used in dual-band GSM/DCS wireless handsets. His work at Agilent covered RF characterization and modeling of microwave transistors, RF IC, and package design. He joined the Department of Electrical and Electronic Engineering, Hong Kong University of Science and Technology (HKUST), Kowloon, Hong Kong, as an Assistant Professor in November 2000 and became an Associate Professor in 2006. He has authored or coauthored over 140 publications in international journals and conference proceedings. At HKUST, his group has carried out research on novel III-nitride device technologies, III-nitride and silicon-based MEMS (microelectromechanical systems), silicon-based RF/microwave passive components, RF packing technology, and microwave filter design.